HHS Public Access

Author manuscript

Neuropharmacology. Author manuscript; available in PMC 2020 November 01.

Published in final edited form as:

Neuropharmacology. 2019 November 01; 158: 107699. doi:10.1016/j.neuropharm.2019.107699.

Prax330 Reduces Persistent and Resurgent Sodium Channel Currents and Neuronal Hyperexcitability of Subiculum Neurons in a Mouse Model of *SCN8A* Epileptic Encephalopathy.

Eric R. Wengert[1,2], **Anusha U. Saga**[1], **Payal S. Panchal**[1], **Bryan S. Barker**[1,2], **Manoj K. Patel**[1,2]

[1]Department of Anesthesiology, University of Virginia Health System, Charlottesville, VA 22908 USA

[2]Neuroscience Graduate Program, University of Virginia Health System, Charlottesville, VA 22908 USA

Abstract

SCN8A epileptic encephalopathy is a severe genetic epilepsy syndrome caused by *de novo* gain-of-function mutations of *SCN8A* encoding the voltage-gated sodium (Na) channel (VGSC) $Na_V1.6$. Therapeutic management is difficult in many patients, leading to uncontrolled seizures and risk of sudden unexpected death in epilepsy (SUDEP). There is a need to develop novel anticonvulsants that can specifically target aberrant Na channel activity associated with *SCN8A* gain-of-function mutations. In this study, we investigate the effects of Prax330, a novel Na channel inhibitor, on the biophysical properties of WT $Na_V1.6$ and the patient mutation p.Asn1768Asp (N1768D) in ND7/23 cells. The effects of Prax330 on persistent (I_{NaP}) and resurgent (I_{NaR}) Na currents and neuronal excitability in subiculum neurons from a knock-in mouse model of the *Scn8a*-N1768D mutation (*Scn8a*$^{D/+}$) were also examined. In ND7/23 cells, Prax330 reduced I_{NaP} currents recorded from cells expressing *Scn8a*-N1768D and hyperpolarized steady-state inactivation curves. Recordings from brain slices demonstrated elevated I_{NaP} and I_{NaR} in subiculum neurons from *Scn8a*$^{D/+}$ mutant mice and abnormally large action potential (AP) burst-firing events in a subset of neurons. Prax330 (1 μM) reduced both I_{NaP} and I_{NaR} and suppressed AP bursts, with smaller effect on AP waveforms that had similar morphology to WT neurons. Prax330 (1 μM) also reduced synaptically-evoked APs in *Scn8a*$^{D/+}$ subiculum neurons but not in WT neurons. Our results highlight the efficacy of targeting I_{NaP} and I_{NaR} and inactivation parameters in controlling subiculum excitability and suggest Prax330 as a promising novel therapy for *SCN8A* epileptic encephalopathy.

Corresponding author: Manoj K. Patel, Ph.D., Department of Anesthesiology, University of Virginia Health System, Charlottesville VA, 22908-0710, USA. Tel: +1 434 924 9693 Fax: +1 434 924 2105, (mkp5u@virginia.edu).

Author Contributions

ERW and MKP designed research. ERW, BSB, PSP and AUS performed experiments. ERW analyzed data. ERW and MKP wrote the manuscript. All authors approved the final version. We thank Praxis Precision Medicine for providing Prax330.

Keywords

Sodium channels; Persistent Sodium Current; Resurgent Sodium Current; Prax330; Subiculum; Epileptic Encephalopathy; *SCN8A*; Action Potentials

1. Introduction

SCN8A epileptic encephalopathy (EIEE13) is caused by *de novo* gain-of-function mutations in the *SCN8A* gene encoding VGSC isoform $Na_V1.6$ (de Kovel et al., 2014; Estacion et al., 2014; Veeramah et al., 2012). Localized predominantly at the axon initial segment (AIS) and nodes of Ranvier, $Na_V1.6$ strongly determines membrane potential and action potential (AP) firing properties of neurons under normal conditions and in disease (Barker et al., 2017; Blumenfeld et al., 2009; Caldwell et al., 2000; Duflocq et al., 2008; Hargus et al., 2013, n.d.; Hu et al., 2009). Patients with *SCN8A* epileptic encephalopathy exhibit seizure onset in infancy leading to motor and cognitive impairment (Larsen et al., 2015; Wagnon and Meisler, 2015).

The first characterized *SCN8A* encephalopathy mutation was p.Asn1768Asp (N1768D) (Veeramah et al., 2012). The patient presented with refractory epilepsy at six months of age, intellectual disability, ataxia, and sudden unexplained death in epilepsy (SUDEP) at 15 years. Biophysical characterization of the mutation in expression systems and neurons revealed a depolarizing shift in the voltage-dependence of steady-state inactivation, an increase in the non-inactivating persistent sodium current (I_{NaP}) after termination of the transient current (I_{NaT}), and an elevated resurgent current (I_{NaR}) (Ottolini et al., 2017; Patel et al., 2016; Veeramah et al., 2012). I_{NaP} has been implicated in setting AP threshold (Deng and Klyachko, 2016), amplifying incoming excitatory and inhibitory synaptic inputs (Hardie and Pearce, 2006; Stafstrom et al., 1985; Stuart and Sakmann, 1995), driving the burst-firing mode of AP firing (Alkadhi and Tian, 1996; Su et al., 2001; Tsuruyama et al., 2013), and orchestrating rhythmogenesis in various neuronal circuits (Dong and Ennis, 2014; Paton et al., 2006; Tazerart et al., 2008; Yamanishi et al., 2018; Zhong et al., 2007). Studies of animal models and human epilepsy tissue have reported increases in I_{NaP} (Barker et al., 2017; Chen et al., 2011; Hargus et al., 2013; Lopez-Santiago et al., 2017; Ottolini et al.,2017; Stafstrom, 2007; Tryba et al., 2011; Vreugdenhil et al., 2004). I_{NaR} also contributes to increased AP frequency and burst firing (Khaliq et al., 2003; Raman et al., 1997; Raman and Bean, 1997). It has therefore been suggested that elevation of I_{NaP} and I_{NaR}, due to expression of mutant VGSC or other modulation of VGSC function, may be a central mechanism contributing to neuronal hyperexcitability associated with seizure initiation (Stafstrom, 2007).

Many clinically available antiepileptic drugs (AEDs) that target VGSCs inhibit I_{NaP}, including phenytoin, carbamazepine, topiramate, and lamotrigine (Alexander and Huguenard, 2014; Colombo et al., 2013; Segal and Douglas, 1997; Spadoni et al., 2002; Sun et al., 2007). For this reason, development of a preferential inhibitor of I_{NaP} could lead to a more efficacious and potentially better tolerated AEDs (Stafstrom, 2007). Prax330 was initially developed as a selective I_{NaP} inhibitor to treat cardiac arrhythmia (Belardinelli et al., 2013; Koltun et al., 2016), however, due its brain permeability and half-life, development of

Prax330 was repurposed as an AED (Belardinelli et al., 2013; Koltun et al., 2016). More recently, Prax330 has been evaluated for efficacy in a number of severe genetic epilepsy syndrome models. *In vivo* studies in *Scn1a*$^{+/-}$, *Scn2a*^{Q54}, *Scn8a*$^{R1872W/+}$, and *Scn8a*$^{D/+}$ mouse models of epileptic encephalopathy revealed that Prax330 is able to potently reduce I_{NaP} and suppress spontaneous AP firing in acutely dissociated hippocampal neurons, normalize CA1 pyramidal AP waveforms, protect against seizures, and extend survival (Anderson et al., 2017, 2014; Baker et al., 2018; Bunton-Stasyshyn et al., 2019).

In order to further investigate the mechanisms by which Prax330 exhibits anticonvulsant activity in the *Scn8a*$^{D/+}$ mouse model of epileptic encephalopathy, we examined the effects of Prax330 on the biophysical properties of the mutant $Na_V1.6$-N1768D in ND7/23 cultured cells and on I_{NaP}, I_{NaR}, and neuronal excitability in subiculum neurons from *Scn8a*$^{D/+}$ mice. Subiculum neurons were chosen because they provide the primary output of the hippocampus and have been previously implicated in epilepsy (Barker et al., 2017; de Guzman et al., 2006; Fujita et al., 2014; Toyoda et al., 2013; Vreugdenhil et al., 2004). In ND7/23 cells, Prax330 reduced I_{NaP} currents in N1768D-expressing cells and caused a leftward shift in inactivation curves of both WT and N1768D channels. Electrophysiological recordings revealed elevated I_{NaP} and I_{NaR} currents and aberrantly large AP-burst waveforms in a subset of *Scn8a*$^{D/+}$ subiculum neurons. Prax330 (1 μM) reduced I_{NaP} and I_{NaR} and attenuated the abnormal AP-burst waveforms in this subset of subiculum neurons without affecting those with normal AP morphology. Synaptically-evoked APs from *Scn8a*$^{D/+}$ subiculum neurons were inhibited by Prax330 (1 μM) while WT neurons were unaffected. These findings suggest that Prax330 preferentially targets aberrant Na channels associated with *SCN8A* mutations and may be useful in the treatment of *SCN8A* epileptic encephalopathy and other forms of genetic and acquired epilepsy.

2. Methods

2.1 ND7/23 Electrophysiology

The introduction of the N1768D mutation into the TTX-resistant $Na_V1.6$ cDNA was previously described (Veeramah et al, 2012). DRG-neuron derived ND7/23 cells (Sigma Aldrich) were grown in a humidified atmosphere of 5% CO_2 and 95% air at 37°C in Dulbecco's Modified Eagle Medium (DMEM 1X) supplemented with 10% FBS, NEAA and Sodium Pyruvate. Cells were plated onto petri dishes 48 hours prior to transfection and transfected for 5 hours in non-supplemented DMEM using Lipofectamine 3000 according to manufacturer instructions (Life Technologies) with 5 μg of $Na_V1.6$ alpha subunit cDNA and 0.5 μg of the fluorescent m-Venus bioreporter. Electrophysiological recordings of fluorescent cells were made 48 hours after transfection.

Whole-cell patch-clamp electrophysiological recordings of sodium currents were carried out as described previously (Barker et al., 2016; Wagnon et al., 2018, 2016). The external recording solution contained in mM: 130 NaCl, 3 KCL, 1 $CaCl_2$, 5 $MgCl_2$, 0.1 $CdCl_2$, 10 HEPES, 30 TEA, 4 4-AP, and 500 nM TTX to block any endogenous Na currents (pH adjusted to 7.4 using NaOH). The osmolality was confirmed to be ~305 mOsm. The intracellular recording solution contained in mM: 140 CsF, 2 $MgCl_2$, 1 EGTA, 10 HEPES, 4 Na_2ATP, 0.3 NaGTP (pH adjusted to 7.2 with CsOH and osmolality adjusted to 300 mOsm).

All experiments were performed at room temperature (22-24°C). Borosilicate recording pipettes were pulled to have resistances of 1.5-3.0 MΩ in recording solution. After achieving the whole-cell configuration, whole-cell capacitance and 75% series resistance were compensated. Currents were amplified, low-pass filtered at 2 kHz, and sampled at 33kHz. Cells were held at −120 mV. The voltage-dependent activation was measured from the current-voltage relationship determined using a 100 ms voltage step to command potentials ranging from −80 to 70 mV at 5 mV increments and conductance as a function of voltage was described by a Boltzmann fit of the data. The average I_{NaP} was taken to be the average current from 60-100 ms after the onset of the voltage step, once the current had reached steady state, and recorded as a percentage of the magnitude of the I_{NaT}. Steady-state inactivation, cells were stepped to pre-pulse potentials ranging from −120 to −10 mV for 500 ms before being stepped to −10 mV to assess channel availability. When calculating steady-state inactivation conductance as a function of voltage, the current of greatest magnitude was determined normalized to 1 and the final sweep which is a continuous step to −10 mV, which does not evoke any I_{NaT}, was set to be 0. The results are well-fit by a single Boltzmann equation as previously described (Barker et al., 2016).

2.2 Brain Slice Preparation

WT and *Scn8a*$^{D/+}$ mice greater than 8 weeks of age were euthanized using isoflurane and decapitated. The brains were rapidly removed and kept in ice-cold (~0°C) artificial cerebrospinal fluid (ACSF) containing in mM: 125 NaCl, 2.5 KCl, 1.25 NaH_2PO_4, 2 $CaCl_2$, 1 $MgCl_2$, 0.5 L-Ascorbic acid, 10 glucose, 25 $NaHCO_3$, and 2 Pyruvate. The ACSF at all stages of the experiment was oxygenated with 95%/5% O_2/CO_2. Horizontal brain sections of 300 μM thickness were cut using a Leica VT1200 vibratome. The slices were placed in 37°C oxygenated ACSF for ~30 minutes and then kept at room temperature.

2.3 Electrophysiology

Brain slices were placed in small chamber continually superfused (~1-2 mL/min) with recording solution warmed to (~32°C). Subiculum pyramidal neurons were visually identified by infra-red video microscopy (Hamamatsu, Shizouka, Japan) using a Zeiss Axioscope microscope. Whole-cell recordings were performed using an Axopatch 700B amplifier (Molecular Devices, pCLAMP 10 software) and were digitized by a Digidata 1322A digitizer (Molecular Devices). Currents were amplified, low-pass filtered at 2 kHz, and sampled at 100 kHz. Borosilicate electrodes were fabricated using a Brown-Flaming puller (Model P1000, Sutter Instruments Co) to have pipette resistances between 2-3.5 MΩ.

2.3.1 I_{NaP} Recordings—I_{NaP} currents were recorded as previously described using a solution containing in mM: 20 NaCl, 130 TEA-Cl, 10 $NaHCO_3$, 1.6 $CaCl_2$, 2 $MgCl_2$, 0.2 $CdCl_2$, and 5 4-AP, and 15 glucose (pH adjusted to 7.4; 305 mOsm) (Ottolini et al., 2017). The pipette solution contained (in mM): 140 CsF, 2 $MgCl_2$, 1 EGTA, 10 HEPES, 4 Na_2ATP, and 0.3 NaGTP (pH adjusted to 7.3, 310 mOsm). Voltage ramps from −100 to −10 at 65 mV/sec led to inward ramp currents with a clear peak near −30 mV. Any cells with ramp currents that escaped voltage-control were discarded and not analyzed. Identical recordings in the presence 500 nM TTX were used to definitively isolate the sodium component of the

ramp current. TTX-subtracted traces were used for calculation of peak inward current and the voltage of half-maximal activation ($V_{1/2}$).

2.3.2 I_{NaR} Recordings—I_{NaR} currents were recorded as previously described using a modified recording solution containing in mM: 100 NaCl, 26 $NaHCO_3$, 19.5 TEA-Cl, 3 KCl, 2 $MgCl_2$, 2 $CaCl_2$, 2 $BaCl_2$, 0.1 $CdCl_2$, 4 4-AP, and 10 glucose (pH of 7.4; 305 mOsm) (Barker et al., 2017). The intracellular solution was the same as that for I_{NaP} recordings. Neurons were held at −100 mV, depolarized to 0 mV for 20 ms and then repolarized to voltages ranging between −100 mV and −20 mV in increments of 10 mV. The peak amplitude of I_{NaR} was calculated as the maximum TTX-sensitive current elicited (typically on the −30 mV step) with the steady-state current subtracted as done previously (Royeck et al., 2008).

2.3.3 AP Recordings—Current clamp recordings were performed with an extracellular recording solution identical to that used in the slicing procedure. The intracellular solution contained in mM: 120 K-gluconate, 10 NaCl, 2 $MgCl_2$, 0.5 K_2EGTA, 10 HEPES, 4 Na_2ATP, 0.3 NaGTP (pH 7.2; osmolarity 290 mOsm). A ramp of depolarizing current 100 pA/sec was used to accurately measure AP threshold which was defined as the membrane potential at which the slope reached 5% of the upstroke velocity (Yamada-Hanff and Bean, 2013). AP amplitude was calculated as the range between threshold and the peak of the AP. A range of depolarizing current injections (−20 to 470 pA in increments of 10 pA) was used to calculate membrane and AP properties. To compare across all neurons, a slow injection of DC current was used to hold neurons at −65 mV throughout the recording. The rheobase was defined as the highest current step injected that did not result in AP firing. Input resistance was calculated using the initial −20 pA step. The upstroke and downstroke velocities were the maximum and minimum of the first derivative of the recorded trace. The AP duration (APD_{50}) was measured as the time duration of the AP measured at the midpoint between the threshold and the peak of the AP. The area under the curve (AUC) of the first AP was calculated relative to AP threshold for each cell. Synaptically-evoked APs were generated through stimulation of the CA1 afferents using a bipolar iridium stimulator (WPI, Sarasota, FL, USA). The stimulus duration was 400 μs and the intensity was adjusted (usually between 1 and 3.2 mA) to evoke APs on successive sweeps with a 10 second inter-sweep interval.

2.4 Drug

Prax330 was provided by Praxis Precision Medicines and was solubilized in DMSO at a stock concentration of 10 mM and stored at −20°C. For all electrophysiology experiments, initial recordings were collected at baseline and then again after ~10 minutes with bath solution containing Prax330. Vehicle control recordings were done in an identical manner without Prax330.

2.5 Data Analysis

All data were analyzed by custom-written MATLAB scripts, or manually with ClampFit. Graphpad software was used for displaying data and for all statistical calculations. All values represent means ± standard error of the mean (S.E.M.) or as individual data points.

Statistical significance was determined using unpaired or paired t-test where appropriate with an alpha set to 0.05 (GraphPad Prism 6.02).

3. Results

3.1 Prax330 inhibits I_{NaP} and modulates inactivation parameters of $Na_V1.6$ currents recorded in ND7/23 cells

We first characterized the effect of Prax330 on WT and N1768D $Na_V1.6$ expressed in ND7/23 cells. Cells were held at −120 mV and stepped to potentials between −80 and 50 mV to examine the current-voltage relationship. Current densities between WT and N1768D cells were not different (WT: −103 ± 22 pA/pF (n=9), N1768D: −45 ± 14 pA/pF (n=7); Figure 1A–D). In agreement with previous studies (Veeramah et al., 2012), a pronounced elevation of I_{NaP} was observed in N1768D transfected cells (Figure 1B, F). I_{NaP} was barely detectable in WT $Na_V1.6$ transfected cells (Figure 1A, E). Prax330 inhibited N1768D-derived I_{NaP} in a dose-dependent manner with an approximate EC_{50} of 625 nM and a Hill slope of 1.5 (Figure 1G). At 1 μM, Prax330 significantly inhibited I_{NaP} by 67% (8.1 ± 1.3% of I_{NaT} before and 3.0 ± 1.1% of I_{NaT} after Prax330; $T(_6)$=3.61; P=0.0112; Figure 1F). Prax330 (1 μM) had no effect on I_{NaT} in WT cells (−103 ± 22 pA/pF at baseline to −84 ± 19 pA/pF after Prax330 treatment; n=9; Figure 1E, I). Prax330 did significantly reduce I_{NaT} in N1768D cells by 49 ± 10% at 300nM ($T(_{14})$= 3.395; P=0.0044; n= 4) and by 41 ± 5% at 1 μM ($T(_{17})$=3.48; P=0.0029; n=7) when compared to vehicle-treated time controls. (Figure 1H, I). These findings suggest that Prax330 shows a particular efficacy toward the N1768D mutation compared to WT.

We assessed the effect of Prax330 (1 μM) on the voltage-dependence of steady-state activation and inactivation (Figure 2; Table 1). Voltage-dependent activation parameters were not different between WT and N1768D transfected cells (Table 1), but steady-state inactivation curves were significantly right-shifted in N1768D cells compared with WT, as previously reported ($T(_{12})$=4.173; P=0.0013; Fig. 2B,D; Table 1) (Veeramah et al., 2012). Left-shifts in activation curves for both WT and N1768D recorded in the presence of Prax330 (1 μM) were not different from shifts observed in vehicle-treated control recordings, indicating that Prax330 has no effect on activation parameters (Figure 2E; Table 1). In contrast, left-shifts in steady-state inactivation after Prax330 (1 μM) treatment for both WT and N1768D cells were significantly larger than that observed in vehicle controls suggesting that Prax330 (1 μM) has an affinity for inactivated channels (P<0.05; Table 1, Figure 2B–J).

3.2 I_{NaP} is accentuated in $Scn8a^{D/+}$ subiculum neurons and is inhibited by Prax330

I_{NaP} was measured in subiculum neurons from acute brain slices obtained from *Scn8a*$^{D/+}$ mice and compared with WT littermates using slow voltage ramps from the holding potential of −100 mV to −10 mV at 65 mV/sec. Maximum I_{NaP} were significantly increased in *Scn8a*$^{D/+}$ subiculum neurons (−261 ± 20 pA; n = 24, 8 mice) compared to WT neurons (−173 ± 15 pA; $T(_{38})$=3.167; P=0.003; n=10, 7 mice; Figure 3A–D). When compared to vehicle-treated controls, Prax330 (1 μM) inhibited both WT (by 48.5 ± 6.3%; n = 10, 4 mice: T=2.497; P=0.0256) and *Scn8a*$^{D/+}$ (by 56.9 ± 5.5%; n = 15, 5 mice: T=3.511;

P=0.0020; Figure 3E). Voltage-dependent activation parameters were not different between Prax330-treated and vehicle-treated neurons (Figure 3F).

3.3 Scn8a$^{D/+}$ subiculum neurons have elevated I_{NaR} which is inhibited by Prax330.

I_{NaR} was also significantly elevated in *Scn8a*$^{D/+}$ brain slice subiculum neurons (−373.1 ± 41 pA; n=20, 7 mice) compared to WT neurons (−229 ± 41 pA; n=15, 8 mice; $T_{(33)}$=2.559; P=0.0153; Fig 4. A, C, E). Compared to vehicle-treated controls (n = 4; 2 mice), Prax330 (1 μM) inhibited I_{NaR} by 37.6 ± 8.3% in *Scn8a*$^{D/+}$ subiculum neurons (n = 16; 5 mice, $T_{(18)}$=2.098; p=0.0495). In contrast, Prax330 (1 μM) had no effect on WT neurons (Figure 4F), suggesting that Prax330 preferentially inhibits I_{NaR} in *Scn8a*$^{D/+}$ neurons.

3.4 Prax330 attenuates aberrant burst AP-firing in Scn8a$^{D/+}$ subiculum neurons.

Aberrant neuronal excitability in AP firing frequency and AP waveform morphology has been reported in medial entorhinal cortex (mEC) and CA1 neurons from *Scn8a*$^{D/+}$ mice (Baker et al., 2018; Lopez-Santiago et al., 2017; Ottolini et al., 2017). Since subiculum neurons provide a major output from the hippocampus and have been implicated in seizure initiation in TLE (Barker et al., 2017; de Guzman et al., 2006; Fujita et al., 2014; Stafstrom, 2005; Toyoda et al., 2013), we examined subiculum neurons from *Scn8a*$^{D/+}$ mice (Figure 5). We found no differences in subiculum neuron AP firing frequencies between *Scn8a*$^{D/+}$ and WT mice (27.9 ± 2.4 Hz; n=18, 7 mice and 27.5 ± 1.7 Hz; n=17, 4 mice respectively). However, a subset of *Scn8a*$^{D/+}$ subiculum neurons (~ 50%) displayed a distinct, all-or-nothing AP burst that was associated with a significantly larger depolarizing event measured by taking the area under the curve (AUC) above AP threshold (1542 ± 112 mV*ms in *Scn8a*$^{D/+}$ compared to 605 ± 74 mV*ms in WT; $T_{(24)}$=7.219; P<0.0001; Fig. 5 A–C,E). The possible bimodal distribution for the AUC led us to separate *Scn8a*$^{D/+}$ neurons into two equal groups (n=9 cells each) based on the magnitude of AUC, *Scn8a*$^{D/+}$-low and high respectively, and examine the relative efficacy of Prax330 on the two groups (Fig. 5 D). Interestingly, Prax330 (1μM) had no significant effect on the burst AUC for WT or *Scn8a*$^{D/+}$-low groups suggesting that *Scn8a*$^{D/+}$ neurons with physiological burst-firing resembling WT are relatively unaffected by Prax330 (Fig. 5 A–B, E). In contrast, *Scn8a*$^{D/+}$-high group neurons were profoundly modulated by Prax330 (1μM), resulting in a significant reduction in the AUC value (1542 ± 112 mV*ms before and 1095 ± 192 mV*ms after treatment with Prax330; $T_{(8)}$=2.327; P=0.0484; Fig 5. C, E). Together these results suggest that Prax330 has a greater effect on *Scn8a*$^{D/+}$ neurons with aberrant firing, potentially due to its effect on I_{NaR} and I_{NaP}, two currents that are known to contribute to burst firing and are increased in amplitude in *Scn8a*$^{D/+}$ subiculum neurons.

3.5 Prax330 rescues hyperpolarized AP thresholds in Scn8a$^{D/+}$ subiculum neurons

Examination of membrane properties revealed that AP thresholds were significantly hyperpolarized in *Scn8a*$^{D/+}$ (−45.6 ± 0.9 mV; n=18, 7 mice) compared to WT mice (−43.2 ± 0.7 mV; n=17 neurons, 4 mice; $T_{(33)}$=2.096; P=0.0438; Fig 6. A–C; Table 2). Notably, Prax330 (1μM) depolarized the threshold voltages in *Scn8a*$^{D/+}$ neurons to voltages observed in WT neurons, thus rescuing a critical determinant of neuronal excitability. Neither resting membrane potential (WT; −63.9 ± 0.6 mV, *Scn8a*$^{D/+}$; −62.9 ± 0.6 mV) nor membrane capacitance (WT; 37.9 ± 5.1 pF, Scn8a$^{D/+}$ 48.5 ± 4.7 pF) were different between WT and

Scn8a$^{D/+}$ neurons. AP amplitude and upstroke velocity were also not different between WT and *Scn8a*$^{D/+}$neurons, but were reduced in response to Prax330 (1μM) for both genotypes, as expected for a Na channel blocker (Table 2). Surprisingly, we observed an increase in input resistance in *Scn8a*$^{D/+}$ neurons after Prax330 treatment (Table 2). Differences observed in rheobase, downstroke velocity, and APD_{50} between *Scn8a*$^{D/+}$ and WT neurons were not modulated by Prax330 (Table 2).

3.6 Prax330 reduces synaptically-evoked APs in Scn8a$^{D/+}$ but not WT neurons.

I_{NaP} currents strongly regulate the propensity for a neuron to initiate an AP in response to incoming synaptic excitation by amplifying synaptic inputs from dendrites (Schwindt and Crill, 1995; Stuart, 1999). Due to effects of Prax330 on I_{NaP}, we examined the ability of Prax330 to modulate synaptically-evoked APs. In WT neurons (n= 9, 4 mice) Prax330 (1 μM) had no effect on synaptically evoked APs (Fig 7. A,C). In striking contrast, Prax330 (1 μM) significantly reduced the number of synaptically-evoked APs from *Scn8a*$^{D/+}$ subiculum neurons (n= 8, 4 mice; $T(_7)$=3.149; P=0.0162; Fig 7. B, C). This effect of Prax330 would significantly dampen the increased network excitability associated with *SCN8A* epileptic encephalopathy (Ottolini et al., 2017).

4. Discussion

In this study, we demonstrate that 1) subiculum neurons from a mouse knock-in model expressing the patient mutation N1768D (*Scn8a*$^{D/+}$) have pro-excitatory firing properties with elevated I_{NaP} and I_{NaR} Na channel currents compared to WT littermates, 2) Prax330, a Na channel inhibitor, modulates inactivation parameters of WT and N1768D $Na_V1.6$ currents, causing hyperpolarizing shifts in inactivation parameters and inhibiting I_{NaP} observed in N1768D cells, 3) in *Scn8a*$^{D/+}$ subiculum neurons *in situ*, Prax330 reduces I_{NaP} and I_{NaR} and selectively suppresses abnormal burst-firing only in high-bursting neurons. These specific effects of Prax330 on Na channel currents, particularly its ability to suppress I_{NaP} and I_{NaR}, could account for its ability to specifically target abnormally large AP bursts in a subset of *Scn8a*$^{D/+}$ subiculum neurons, while having little effect on normal bursting *Scn8a*$^{D/+}$ neurons or WT neurons, and for its anticonvulsant activity in *Scn8a*$^{D/+}$ mice (Baker et al., 2018).

Elevated I_{NaP} has been implicated in facilitating neuronal hyperexcitability associated with epilepsy. Many gain-of-function mutations in $Na_V1.1$, $Na_V1.2$, $Na_V1.3$, and $Na_V1.6$ display an increased I_{NaP} (Blanchard et al., 2015; de Kovel et al., 2014; George, 2004; Holland et al., 2008; Liao et al., 2010; Ottolini et al., 2017; Rhodes et al., 2004; Veeramah et al., 2012; Wagnon and Meisler, 2015; Zaman et al., 2018). Increased I_{NaP} has been reported in animal models of temporal lobe epilepsy and in human epilepsy patients (Agrawal et al., 2003; Barker et al., 2017; Chen et al., 2011; Hargus et al., 2013; Stafstrom, 2007; Vreugdenhil et al., 2004). Increased I_{NaP} induces aberrant neuronal excitability, producing large burst AP events, leading to seizures in rodents (Alkadhi and Tian, 1996; Mantegazza et al., 1998; Otoom et al., 2006; Otoom and Alkadhi, 2000), and suppression of I_{NaP} by AEDs is considered an important mechanism of action (Stafstrom, 2007). Consistent with these observations, preferential inhibitors of I_{NaP} have shown promise in animal models of

epilepsy (Anderson et al., 2014; Romettino et al., 1991; Urbani and Belluzzi, 2000). Prax330 was originally developed as an antiarrhythmic drug due to its ability to target I_{NaP} generated by the cardiac Na channel, $Na_v1.5$ (Belardinelli et al., 2013; Potet et al., 2016; Sicouri et al., 2013). In this study, we demonstrate that Prax330 is a potent inhibitor of neuronal I_{NaP}, with effects not only on the mutant $Na_v1.6$-N1768D channel expressed in a neuron-derived cell line, but also on subiculum neurons *in situ*. Since I_{NaP} is thought to provide sustained depolarization after an initiated AP and amplify synaptic inputs from distal dendrites to facilitate repetitive and/or burst-firing of APs, suppression of these currents is predicted to suppress epileptiform burst firing (Harvey et al., 2006; Schwindt and Crill, 1995; Stuart, 1999; Stuart and Sakmann, 1995; Yamada-Hanff and Bean, 2013). In agreement with this prediction, Prax330 normalized the AP-burst waveform in *Scn8a*$^{D/+}$ CA1 pyramidal neurons without an effect on WT AP firing (Baker et al., 2018). Here we show that Prax330 is particularly effective at modulating subiculum neurons with large, abnormal AP waveforms, and has little effect on APs that did not display epileptiform morphology. We suggest that these aberrantly firing neurons likely exhibited larger I_{NaP} and/or I_{NaR} currents, accounting for their sustained depolarization and prolonged neuronal excitation. Selective inhibition of epileptiform neurons enhances the therapeutic potential of Prax330 and could reduce unwanted side effects.

The I_{NaR} is a slow inactivating depolarizing current that can contribute to increased AP frequency and burst firing by providing additional depolarization during the falling phase of an AP (Khaliq et al., 2003; Raman et al., 1997; Raman and Bean, 1997). Increases in I_{NaR} have been reported in animals models of epilepsy and are also considered therapeutic targets in epilepsy (Hargus et al., 2013; Jarecki et al., 2010; Khaliq et al., 2003; Patel et al., 2016). Here we show that *Scn8a*$^{D/+}$ subiculum neurons have elevated I_{NaR} that are suppressed by Prax330. Recent studies indicate that inhibition of I_{NaR} is an important mechanism of action of cannabidiol, a compound with promise in treating different types of epilepsy including genetic epilepsies (Devinsky et al., 2017, 2016; Kaplan et al., 2017; Khan et al., 2018; Patel et al., 2016). However, recent evidence suggests that cannabidiol also inhibits the transient sodium current making these studies inconclusive regarding the specific role of I_{NaR} in epilepsy (Ghovanloo et al., 2018). We evaluated the effects of Prax330 on subiculum neurons because they provide a major output from the hippocampus proper and are an important anatomical site affecting seizure initiation (Fujita et al., 2014; Toyoda et al., 2013). It has been proposed that synaptic connection from CA1 neurons to subiculum neurons is reorganized in epilepsy leading to increased excitation of subiculum neurons (Cavazos et al., 2004; de Guzman et al., 2006). Subiculum neurons from epileptic rodents have elevated I_{NaP} and I_{NaR} leading to hyperexcitability (Barker et al., 2017; de Guzman et al., 2006; Wellmer et al., 2002). Similarly, Vreugdenhil and colleagues demonstrated that I_{NaP} is elevated in a subset of subiculum neurons from human epilepsy patients (Vreugdenhil et al., 2004). Only a subset (~50 %) of the recorded neurons had elevated I_{NaP}, leading to the hypothesis of two distinct neuronal populations distinguished by I_{NaP} levels. Our data are consistent a similar heterogeneity in *Scn8a*$^{D/+}$ subiculum neurons.

Prax330 has shown efficacy in animal models of epileptic encephalopathy including the *Scn1a*$^{+/-}$, *Scn2a*^{Q54}, *Scn8a*$^{D/+}$ and most recently the *Scn8a*$^{R1872W/+}$ models of *SCN8A* encephalopathy, providing support for the view that disrupted inactivation of Na channels

can contribute generally to epileptic encephalopathies (Anderson et al., 2017, 2014; Baker et al., 2018). The efficacy of Prax330 in the *Scn1a*$^{+/-}$ model of Dravet Syndrome with reduced Scn1a activity is surprising, and suggests that inhibiting $Na_V1.6$ and associated I_{NaP} and I_{NaR} with Prax330 differentially impacts the excitability of pyramidal neurons and inhibitory interneurons (Anderson et al., 2017), potentially resetting the network imbalance. Alternatively, the mechanism could be indirect since chronic dosing with Prax330 was shown to reduced $Na_v1.6$ protein expression (Anderson et al., 2017). The fact that Prax330 is efficacious in two distinct mouse models of epileptic encephalopathy highlights the uniqueness of Prax330 among other Na channel blockers and could be due to its preferential targeting of I_{NaP} and I_{NaR} over I_{NaT}. Further mechanistic studies are warranted to clarify the precise molecular mechanisms of Prax330.

5. Conclusion

Scn8a$^{D/+}$ subiculum neurons have elevated I_{NaP} and I_{NaR} currents which lead to abnormal burst-firing of APs and is likely to contribute to network hyperexcitability associated with seizure generation. In ND7/23 cells, we demonstrate that Prax330 is able to reduce I_{NaP} and modulate steady-state inactivation of $Na_V1.6$ Na channel currents. In brain slice preparations, we show that Prax330 is able to block both I_{NaP} and I_{NaR}, to reduce the magnitude of AP bursting in neurons with abnormal AP burst waveforms, and to inhibit synaptically-evoked APs from *Scn8a*$^{D/+}$ subiculum neurons. Taken together, our data support efforts to develop new therapeutics that preferentially inhibit I_{NaP} and I_{NaR} currents. Development of candidate therapeutics with these characteristics could prove highly effective in the treatment of *SCN8A* epileptic encephalopathy and other types of epilepsy.

Acknowledgements:

We thank Dr. Miriam Meisler for providing the *Scn8a*$^{D/+}$ mutant mice and the N1768D clone and for helpful comments on the manuscript. This work was supported by National Institutes of Health/National Institute for Neurological Disorders and Stroke grant (NINDS) R01NS103090 to MKP, and University of Virginia's Robert R. Wagner Fellowship to ERW.

Disclosure of Conflict of Interest

MKP has received prior support from Praxis Precision Medicines. The remaining authors have no conflicts of interest. We confirm that we have read the ethical guidelines supplied by the Journal and that this report is consistent with those guidelines.

Abbreviations:

Na	Sodium
I_{NaT}	Transient current
I_{NaP}	Persistent Sodium Current
I_{NaR}	Resurgent Sodium Current
AIS	Axon initial segment
AP	Action potential

REFERENCES

Agrawal N, Alonso A, Ragsdale DS, 2003 Increased Persistent Sodium Currents in Rat Entorhinal Cortex Layer V Neurons in a Post-Status Epilepticus Model of Temporal Lobe Epilepsy. Epilepsia. 10.1111/j.0013-9580.2003.23103.x

Alexander A, Huguenard J, 2014 Lamotrigine suppresses thalamic epileptiform oscillations via a blockade of the persistent sodium current. Epilepsy Curr.

Alkadhi KA, Tian LM, 1996 Veratridine-enhanced persistent sodium current induces bursting in CA1 pyramidal neurons. Neuroscience. 10.1016/0306-4522(95)00488-2

Anderson LL, Hawkins NA, Thompson CH, Kearney JA, George AL, 2017 Unexpected Efficacy of a Novel Sodium Channel Modulator in Dravet Syndrome. Sci. Rep 10.1038/s41598-017-01851-9

Anderson LL, Thompson CH, Hawkins NA, Nath RD, Petersohn AA, Rajamani S, Bush WS, Frankel WN, Vanoye CG, Kearney JA, George AL Jr, George AL, 2014 Antiepileptic Activity of Preferential Inhibitors of Persistent Sodium Current. Epilepsia 55, 1274–1283. 10.1111/epi.12657 [PubMed: 24862204]

Baker EM, Thompson CH, Hawkins NA, Wagnon JL, Wengert ER, Patel MK, George AL, Meisler MH, Kearney JA, 2018 The novel sodium channel modulator GS-458967 (GS967) is an effective treatment in a mouse model of SCN8A encephalopathy. Epilepsia 59, 1166–1176. 10.1111/epi.14196 [PubMed: 29782051]

Barker BS, Nigam A, Ottolini M, Gaykema RP, Hargus NJ, Patel MK, 2017 Pro-excitatory alterations in sodium channel activity facilitate subiculum neuron hyperexcitability in temporal lobe epilepsy. Neurobiol. Dis 10.1016/j.nbd.2017.08.018

Barker BS, Ottolini M, Wagnon JL, Hollander RM, Meisler MH, Patel MK, 2016 The SCN8A encephalopathy mutation p.Ile1327Val displays elevated sensitivity to the anticonvulsant phenytoin. Epilepsia. 10.1111/epi.13461

Belardinelli L, Liu G, Smith-Maxwell C, Wang W-Q, El-Bizri N, Hirakawa R, Karpinski S, Hong Li C, Hu L, Li X-J, Crumb W, Wu L, Koltun D, Zablocki J, Yao L, Dhalla AK, Rajamani S, Shryock JC, 2013 A Novel, Potent, and Selective Inhibitor of Cardiac Late Sodium Current Suppresses Experimental Arrhythmias. J. Pharmacol. Exp. Ther 10.1124/jpet.112.198887

Blanchard MG, Willemsen MH, Walker JB, Dib-Hajj SD, Waxman SG, Jongmans MCJ,Kleefstra T, van de Warrenburg BP, Praamstra P, Nicolai J, Yntema HG, Bindels RJM, Meisler MH, Kamsteeg EJ, 2015 De novo gain-of-function and loss-of-function mutations of SCN8A in patients with intellectual disabilities and epilepsy. J. Med. Genet 10.1136/jmedgenet-2014-102813

Blumenfeld H, Lampert A, Klein JP, Mission J, Chen MC, Rivera M, Dib-Hajj S, Brennan AR, Hains BC, Waxman SG, 2009 Role of hippocampal sodium channel Nav1.6 in kindling epileptogenesis. Epilepsia. 10.1111/j.1528-1167.2008.01710.x

Bunton-Stasyshyn RKA, Wagnon JL, Wengert ER, Barker BS, Faulkner A, Wagley PK, Bhatia K, Jones JM, Maniaci MR, Parent JM, Goodkin HP, Patel MK, Meisler MH, 2019 Prominent role of forebrain excitatory neurons in SCN8A encephalopathy. Brain awy324–awy324.

Caldwell JH, Schaller KL, Lasher RS, Peles E, Levinson SR, 2000 Sodium channel Nav1.6 is localized at nodes of Ranvier, dendrites, and synapses. Proc. Natl. Acad. Sci 10.1073/pnas.090034797

Cavazos JE, Jones SM, Cross DJ, 2004 Sprouting and synaptic reorganization in the subiculum and CA1 region of the hippocampus in acute and chronic models of partial-onset epilepsy. Neuroscience. 10.1016/j.neuroscience.2004.04.014

Chen S, Su H, Yue C, Remy S, Royeck M, Sochivko D, Opitz T, Beck H, Yaari Y, 2011 . An increase in persistent sodium current contributes to intrinsic neuronal bursting after status epilepticus. J. Neurophysiol 10.1152/jn.00184.2010

Colombo E, Franceschetti S, Avanzini G, Mantegazza M, 2013 Phenytoin Inhibits the Persistent Sodium Current in Neocortical Neurons by Modifying Its Inactivation Properties. PLoS One. 10.1371/journal.pone.0055329

de Guzman P, Inaba Y, Biagini G, Baldelli E, Mollinari C, Merlo D, Avoli M, 2006 Subiculum network excitability is increased in a rodent model of temporal lobe epilepsy. Hippocampus. 10.1002/hipo.20215

de Kovel CGF, Meisler MH, Brilstra EH, van Berkestijn FMC, Slot R van t., van Lieshout S, Nijman IJ, O'Brien JE, Hammer MF, Estacion M, Waxman SG, Dib-Hajj SD, Koeleman BPC, 2014 Characterization of a de novo SCN8A mutation in a patient with epileptic encephalopathy. Epilepsy Res. 10.1016/j.eplepsyres.2014.08.020

Deng PY, Klyachko VA, 2016 Increased Persistent Sodium Current Causes Neuronal Hyperexcitability in the Entorhinal Cortex of Fmr1 Knockout Mice. Cell Rep 10.1016/j.celrep.2016.08.046

Devinsky O, Cross JH, Laux L, Marsh E, Miller I, Nabbout R, Scheffer IE, Thiele EA, Wright S 2017 Trial of Cannabidiol for Drug-Resistant Seizures in the Dravet Syndrome. N. Engl. J. Med 376, 2011–2020. 10.1056/NEJMoa1611618 [PubMed: 28538134]

Devinsky O, Marsh E, Friedman D, Thiele E, Laux L, Sullivan J, Miller I, Flamini R, Wilfong A, Filloux F, Wong M, Tilton N, Bruno P, Bluvstein J, Hedlund J, Kamens R, Maclean J, Nangia S, Singhal NS, Wilson CA, Patel A, Cilio MR, 2016 Cannabidiol in patients with treatment-resistant epilepsy: an open-label interventional trial. Lancet Neurol. 15, 270–278. 10.1016/S1474-4422(15)00379-8 [PubMed: 26724101]

Dong H-W, Ennis M, 2014 Activation of group I metabotropic glutamate receptors enhances persistent sodium current and rhythmic bursting in main olfactory bulb external tufted cells. J. Neurophysiol 10.1152/jn.00696.2013

Duflocq A, Le Bras B, Bullier E, Couraud F, Davenne M, 2008 Nav1.1 is predominantly expressed in nodes of Ranvier and axon initial segments. Mol. Cell. Neurosci 10.1016/j.mcn.2008.06.008

Estacion M, O'Brien JE, Conravey A, Hammer MF, Waxman SG, Dib-Hajj SD, Meisler MH, 2014 A novel de novo mutation of SCN8A (Nav1.6) with enhanced channel activation in a child with epileptic encephalopathy. Neurobiol. Dis 10.1016/j.nbd.2014.05.017

Fujita S, Toyoda I, Thamattoor AK, Buckmaster PS, 2014 Preictal Activity of Subicular, CA1, and Dentate Gyrus Principal Neurons in the Dorsal Hippocampus before Spontaneous Seizures in a Rat Model of Temporal Lobe Epilepsy. J. Neurosci 34, 16671. [PubMed: 25505320]

George AL, 2004 Molecular basis of inherited epilepsy. Arch. Neurol 10.1001/archneur.61.4.473

Ghovanloo M-R, Shuart NG, Mezeyova J, Dean RA, Ruben PC, Goodchild SJ, 2018 Inhibitory effects of cannabidiol on voltage-dependent sodium currents. J. Biol. Chem 293, 16546–16558. 10.1074/jbc.RA118.004929 [PubMed: 30219789]

Hardie JB, Pearce RA, 2006 Active and Passive Membrane Properties and Intrinsic Kinetics Shape Synaptic Inhibition in Hippocampal CA1 Pyramidal Neurons. J. Neurosci 10.1523/JNEUROSCI.0547-06.2006

Hargus NJ, Nigam A, Bertram EH, Patel MK, 2013 Evidence for a role of Nav1.6 in facilitating increases in neuronal hyperexcitability during epileptogenesis. J. Neurophysiol 110, 1144–1157. 10.1152/jn.00383.2013 [PubMed: 23741036]

Hargus NJ, Nigam A, Bertram EH Iii, Patel MK, n.d. Evidence for a role of Na v 1.6 in facilitating increases in neuronal hyperexcitability during epileptogenesis.

Harvey PJ, Li Y., Li X, Bennett DJ, 2006 Persistent Sodium Currents and Repetitive Firing in Motoneurons of the Sacrocaudal Spinal Cord of Adult Rats. J. Neurophysiol 96, 1141–1157. 10.1152/jn.00335.2005 [PubMed: 16282206]

Holland KD, Kearney JA, Glauser TA, Buck G, Keddache M, Blankston JR, Glaaser IW, Kass RS, Meisler MH, 2008 Mutation of sodium channel SCN3A in a patient with cryptogenic pediatric partial epilepsy. Neurosci. Lett 10.1016/j.neulet.2007.12.064

Hu W, Tian C, Li T, Yang M, Hou H, Shu Y, 2009 Distinct contributions of Na v 1.6 and Na v 1.2 in action potential initiation and backpropagation. Nat. Publ. Gr 12 10.1038/nn.2359

Jarecki BW, Piekarz AD, Jackson JO II, Cummins TR, 2010 Human voltage-gated sodium channel mutations that cause inherited neuronal and muscle channelopathies increase resurgent sodium currents. J. Clin. Invest 120, 369–378. 10.1172/JCI40801 [PubMed: 20038812]

Kaplan JS, Stella N, Catterall WA, Westenbroek RE, 2017 Cannabidiol attenuates seizures and social deficits in a mouse model of Dravet syndrome. Proc. Natl. Acad. Sci 114, 11229. [PubMed: 28973916]

Khaliq ZM, Gouwens NW, Raman IM, 2003 The Contribution of Resurgent Sodium Current to High-Frequency Firing in Purkinje Neurons: An Experimental and Modeling Study. J. Neurosci 23, 4899. [PubMed: 12832512]

Khan AA, Shekh-Ahmad T, Khalil A, Walker MC, Ali AB, 2018 Cannabidiol exerts antiepileptic effects by restoring hippocampal interneuron functions in a temporal lobe epilepsy model. Br. J. Pharmacol 10.1111/bph.14202

Koltun DO, Parkhill EQ, Elzein E, Kobayashi T, Notte GT, Kalla R, Jiang RH, Li X, Perry TD, Avila B, Wang WQ, Smith-Maxwell C, Dhalla AK, Rajamani S, Stafford B, Tang J, Mollova N, Belardinelli L, Zablocki JA, 2016 Discovery of triazolopyridine GS-458967, a late sodium current inhibitor (Late INai) of the cardiac NaV 1.5 channel with improved efficacy and potency relative to ranolazine. Bioorganic Med. Chem. Lett. 10.1016/j.bmcl.2016.03.101

Larsen J, Carvill GL, Gardella E, Kluger G, Schmiedel G, Barisic N, Depienne C, Brilstra E, Mang Y, Nielsen JEK, Kirkpatrick M, Goudie D, Goldman R, Jähn JA, Jepsen B, Gill D, Döcker M, Biskup S, McMahon JM, Koeleman B, Harris M, Braun K, de Kovel CGF, Marini C, Specchio N, Djémié T, Weckhuysen S, Tommerup N, Troncoso M, Troncoso L, Bevot A, Wolff M, Hjalgrim H, Guerrini R, Scheffer IE, Mefford HC, Møller RSP, ‡On behalf of the EuroEPINOMICS R E S Consortium C R, 2015 The phenotypic spectrum of SCN8A encephalopathy. Neurology 84, 480–489. 10.1212/WNL.0000000000001211 [PubMed: 25568300]

Liao Y, Anttonen AK, Liukkonen E, Gaily E, Maljevic S, Schubert S, Bellan-Koch A, Petrou S, Ahonen VE, Lerche H, Lehesjoki AE, 2010 SCN2A mutation associated with neonatal epilepsy, late-onset episodic ataxia, myoclonus, and pain. Neurology. 10.1212/WNL.0b013e3181f8812e

Lopez-Santiago LF, Yuan Y, Wagnon JL, Hull JM, Frasier CR, O'Malley HA, Meisler MH, Isom LL, 2017 Neuronal hyperexcitability in a mouse model of *SCN8A* epileptic encephalopathy. Proc. Natl. Acad. Sci 10.1073/pnas.1616821114

Mantegazza M, Franceschetti S, Avanzini G, 1998 Anemone toxin (ATX II)-induced increase in persistent sodium current: effects on the firing properties of rat neocortical pyramidal neurones. J. Physiol 507, 105–116. 10.1111/j.1469-7793.1998.105bu.x [PubMed: 9490824]

Otoom SA, Alkadhi KA, 2000 Epileptiform activity of veratridine model in rat brain slices: effects of antiepileptic drugs. Epilepsy Res. 38, 161–170. [PubMed: 10642044]

Otoom SA, Handu SS, Wazir JF, James H, Sharma PR, Hasan ZA, Sequeira RP, 2006 Veratridine-induced wet dog shake behaviour and apoptosis in rat hippocampus. Basic Clin. Pharmacol. Toxicol. 10.1111/j.1742-7843.2006.pto_339.x

Ottolini M, Barker BS, Gaykema RP, Meisler MH, Patel MK, 2017 Aberrant Sodium Channel Currents and Hyperexcitability of Medial Entorhinal Cortex Neurons in a Mouse Model of *SCN8A* Encephalopathy. J. Neurosci 10.1523/JNEUROSCI.2709-16.2017

Patel RR, Barbosa C, Brustovetsky T, Brustovetsky N, Cummins TR, 2016 Aberrant epilepsy-associated mutant Nav1.6 sodium channel activity can be targeted with cannabidiol. Brain. 10.1093/brain/aww129

Paton JFR, Abdala APL, Koizumi H, Smith JC, St-John WM, 2006 Respiratory rhythm generation during gasping depends on persistent sodium current. Nat. Neurosci 10.1038/nn1650

Potet F, Vanoye CG, George AL, 2016 Use-Dependent Block of Human Cardiac Sodium Channels by GS967. Mol. Pharmacol 10.1124/mol.116.103358

Raman IM, Bean BP, 1997 Resurgent Sodium Current and Action Potential Formation in Dissociated Cerebellar Purkinje Neurons. J. Neurosci 17, 4517. [PubMed: 9169512]

Raman IM, Sprunger LK, Meisler MH, Bean BP, 1997 Altered subthreshold sodium currents and disrupted firing patterns in Purkinje neurons of Scn8a mutant mice. Neuron. 10.1016/S0896-6273(00)80969-1

Rhodes TH, Lossin C, Vanoye CG, Wang DW, George AL, 2004 Noninactivating voltage-gated sodium channels in severe myoclonic epilepsy of infancy. Proc. Natl. Acad. Sci. U. S. A 101, 11147. [PubMed: 15263074]

Romettino S, Lazdunski M, Gottesmann C, 1991 ee ar Eur. J. Pharmacol 199, 371–373. [PubMed: 1915583]

Royeck M, Horstmann M-T, Remy S, Reitze M, Yaari Y, Beck H, 2008 Role of Axonal NaV1.6 Sodium Channels in Action Potential Initiation of CA1 Pyramidal Neurons. J. Neurophysiol 10.1152/jn.90332.2008

Schwindt PC, Crill WE, 1995 Amplification of Synaptic Current by Persistent Sodium Conductance in Apical Dendrite of Neocortical Neurons. JOURNAL OF NEUROPHYSIOLOGY RAPID Publ. 74.

Segal MM, Douglas AF, 1997 Late Sodium Channel Openings Underlying Epileptiform Activity Are Preferentially Diminished by the Anticonvulsant Phenytoin. J. Neurophysiol 77, 3021–3034. 10.1152/jn.1997.77.6.3021 [PubMed: 9212254]

Sicouri S, Belardinelli L, Antzelevitch C, 2013 Antiarrhythmic effects of the highly selective late sodium channel current blocker GS-458967. Hear. Rhythm 10, 1036–1043. 10.1016/j.hrthm.2013.03.023

Spadoni F, Hainsworth AH, Mercuri NB, Caputi L, Martella G, Lavaroni F, Bernardi G, Stefani A, 2002 Lamotrigine derivatives and riluzole inhibit INa,P in cortical neurons. Neuroreport. 10.1097/00001756-200207020-00019

Stafstrom CE, 2007 Persistent Sodium Current and Its Role in Epilepsy. Epilepsy Curr. 10.1111/j.1535-7511.2007.00156.x

Stafstrom CE, 2005 The Role of the Subiculum in Epilepsy and Epileptogenesis. Epilepsy Curr. 10.1111/j.1535-7511.2005.00049.x

Stafstrom CE, Schwindt PC, Chubb MC, Grill WE, 1985 Properties of Penistent Sodium Conductance and Calcium Conductance of Layer V Neurons From Cat Sensorimotor Cortex In Vitro. J. Neurophysiol, 53.

Stuart G, 1999 Voltage–activated sodium channels amplify inhibition in neocortical pyramidal neurons. Nat. Neurosci 2, 144. [PubMed: 10195198]

Stuart G, Sakmann B, 1995 Amplification of EPSPs by axosomatic sodium channels in neocortical pyramidal neurons. Neuron. 10.1016/0896-6273(95)90095-0

Su H, Alroy G, Kirson ED, Yaari Y, 2001 Extracellular Calcium Modulates Persistent Sodium Current-Dependent Burst-Firing in Hippocampal Pyramidal Neurons. J. Neurosci 21, 4173. [PubMed: 11404402]

Sun GC, Werkman TR, Battefeld A, Clare JJ, Wadman WJ, 2007 Carbamazepine and topiramate modulation of transient and persistent sodium currents studied in HEK293 cells expressing the Nav1.3 α-subunit. Epilepsia. 10.1111/j.1528-1167.2007.01001.x

Tazerart S, Vinay L, Brocard F, 2008 The Persistent Sodium Current Generates Pacemaker Activities in the Central Pattern Generator for Locomotion and Regulates the Locomotor Rhythm. J. Neurosci 10.1523/JNEUROSCI.1437-08.2008

Toyoda I, Bower MR, Leyva F, Buckmaster PS, 2013 Early Activation of Ventral Hippocampus and Subiculum during Spontaneous Seizures in a Rat Model of Temporal Lobe Epilepsy. J. Neurosci 33, 11100. [PubMed: 23825415]

Tryba AK, Kaczorowski CC, Ben-Mabrouk F, Elsen FP, Lew SM, Marcuccilli CJ, 2011 Rhythmic intrinsic bursting neurons in human neocortex obtained from pediatric patients with epilepsy. Eur. J. Neurosci 34 10.1111/j.1460-9568.2011.07746.x

Tsuruyama K, Hsiao C-F, Chandler SH, 2013 Participation of a persistent sodium current and calcium-activated nonspecific cationic current to burst generation in trigeminal principal sensory neurons. J. Neurophysiol 10.1152/jn.00410.2013

Urbani A, Belluzzi O, 2000 Riluzole inhibits the persistent sodium current in mammalian CNS neurons. Eur. J. Neurosci 10.1046/j.1460-9568.2000.00242.x

Veeramah KR, O'Brien JE, Meisler MH, Cheng X, Dib-Hajj SD, Waxman SG, Talwar D, Girirajan S, Eichler EE, Restifo LL, Erickson RP, Hammer MF, 2012 De novo pathogenic SCN8A mutation identified by whole-genome sequencing of a family quartet affected by infantile epileptic encephalopathy and SUDEP. Am. J. Hum. Genet 10.1016/j.ajhg.2012.01.006

Vreugdenhil M, Hoogland G, Van Veelen CWM, Wadman WJ, 2004 Persistent sodium current in subicular neurons isolated from patients with temporal lobe epilepsy. Eur. J. Neurosci 19, 2769–2778. 10.1111/j.1460-9568.2004.03400.x [PubMed: 15147310]

Wagnon JL, Barker BS, Hounshell JA, Haaxma CA, Shealy A, Moss T, Parikh S, Messer RD, Patel MK, Meisler MH, 2016 Pathogenic mechanism of recurrent mutations of SCN8A in epileptic encephalopathy. Ann. Clin. Transl. Neurol 10.1002/acn3.276

Wagnon JL, Meisler MH, 2015 Recurrent and non-recurrent mutations of SCN8A in epileptic encephalopathy. Front. Neurol 10.3389/fneur.2015.00104

Wagnon JL, Mencacci NE, Barker BS, Wengert ER, Bhatia KP, Balint B, Carecchio M, Wood NW, Patel MK, Meisler MH, 2018 Partial loss-of-function of sodium channel SCN8A in familial isolated myoclonus. Hum. Mutat 10.1002/humu.23547

Wellmer J, Su H, Beck H, Yaari Y, 2002 Long-lasting modification of intrinsic discharge properties in subicular neurons following status epilepticus. Eur. J. Neurosci 10.1046/j.1460-9568.2002.02086.x

Yamada-Hanff J, Bean BP, 2013 Persistent Sodium Current Drives Conditional Pacemaking in CA1 Pyramidal Neurons under Muscarinic Stimulation. J. Neurosci 10.1523/JNEUROSCI.0577-13.2013

Yamanishi T, Koizumi H, Navarro MA, Milescu LS, Smith JC, 2018 Kinetic properties of persistent Na + current orchestrate oscillatory bursting in respiratory neurons. J. Gen. Physiol 10.1085/jgp.201812100

Zaman T, Helbig I, Božović IB, DeBrosse SD, Bergqvist AC, Wallis K, Medne L, Maver A, Peterlin B, Helbig KL, Zhang X, Goldberg EM, 2018 Mutations in SCN3A cause early infantile epileptic encephalopathy. Ann. Neurol 83, 703–717. 10.1002/ana.25188 [PubMed: 29466837]

Zhong G, Masino MA, Harris-Warrick RM, 2007 Persistent Sodium Currents Participate in Fictive Locomotion Generation in Neonatal Mouse Spinal Cord. J. Neurosci 10.1523/JNEUROSCI.0124-07.2007

Highlights

- Patient mutation *SCN8A*-N1768D produces elevated persistent Na current that is inhibited by Prax330.
- Pro-excitatory depolarizing shifts in N1768D steady-state inactivation curves are rescued by Prax330.
- *Scn8a*$^{D/+}$ subiculum neurons expressing the N1768D mutation have elevated persistent and resurgent Na currents.
- Prax330 attenuates both persistent and resurgent Na currents of *Scn8a*$^{D/+}$ subiculum neurons.
- Prax330 normalizes hyperpolarized threshold and suppresses aberrant bursting in *Scn8a*$^{D/+}$ neurons.
- Prax330 reduces synaptically-evoked action potentials in neurons from *Scn8a*$^{D/+}$, but not WT, mice.

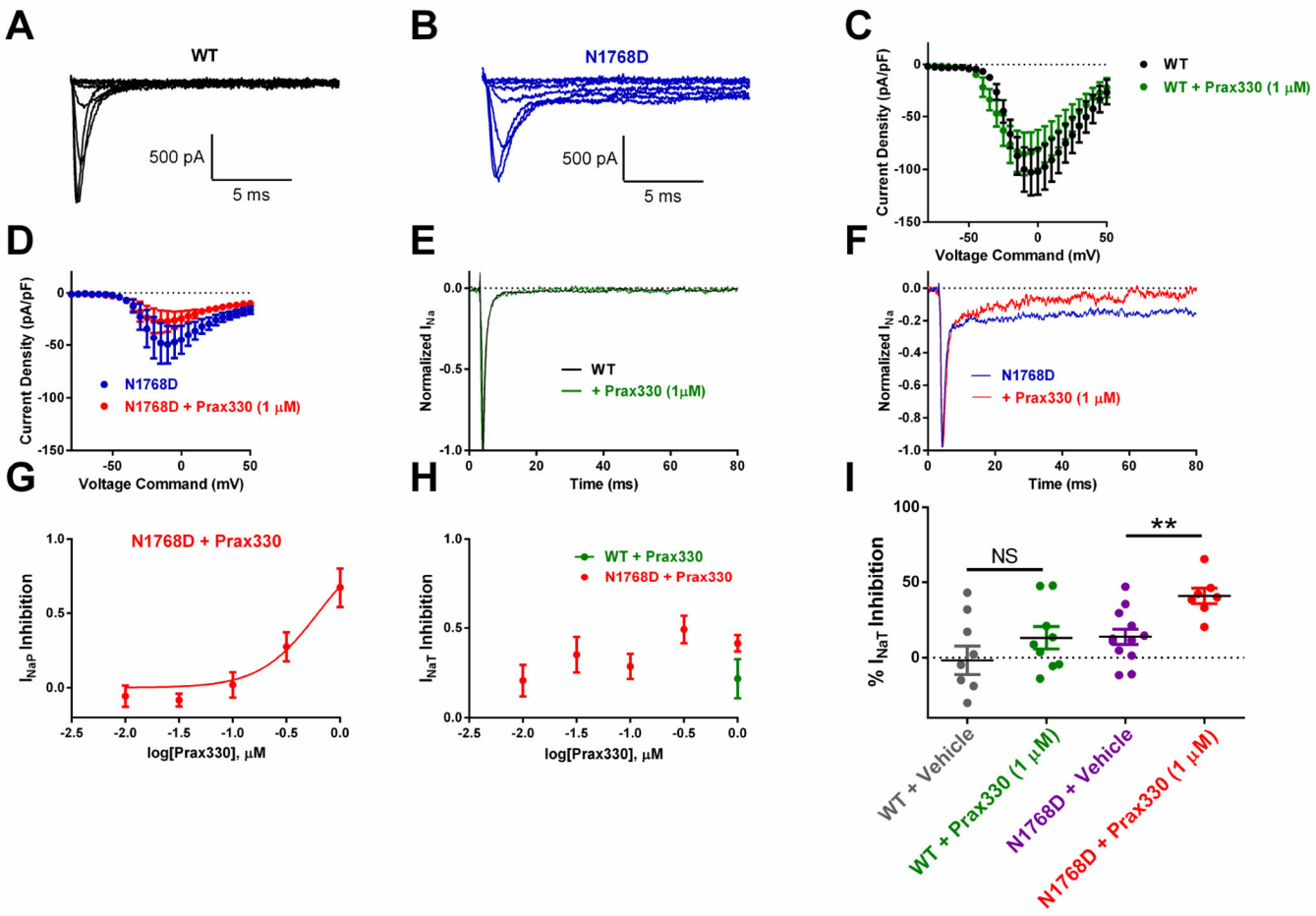

Figure 1. Prax330 inhibits N1768D-derived I_{NaP} in $Na_V1.6$-expressing cells.

A-B. Families of $Na_V1.6$ channel current traces for WT- (**A**) and N1768D- (**B**) expressing ND7/23 cells. **C.** Current/voltage relationship for WT $Na_V1.6$ channel current density before (black) and after (green) treatment with Prax330 (1 μM). **D.** Current/voltage relationship for N1768D $Na_V1.6$ channel current density before (blue) and after (red) treatment with Prax330 (1 μM). **E.** Example normalized trace for WT before (black) and after (green) Prax330 (1 μM) treatment. **F.** Example normalized trace for N1768D before (blue) and after (red) treatment with Prax330 (1 μM). **G.** Dose-response curve for Prax330 on N1768D I_{NaP} (EC_{50} of 625 nM). **H.** Dose-response effect of Prax330 on I_{NaT}. **I.** Scatter plot showing effects of vehicle (gray; n=9) and Prax330 (1 μM; green; n=9) on WT I_{NaT} and vehicle (purple; n=12) or Prax330 (1 μM; red; n=7) on N1768D I_{NaT}. Holding potential was −120 mV for all protocols. Data shown as individual values and/or mean ± SEM. **P<0.01.

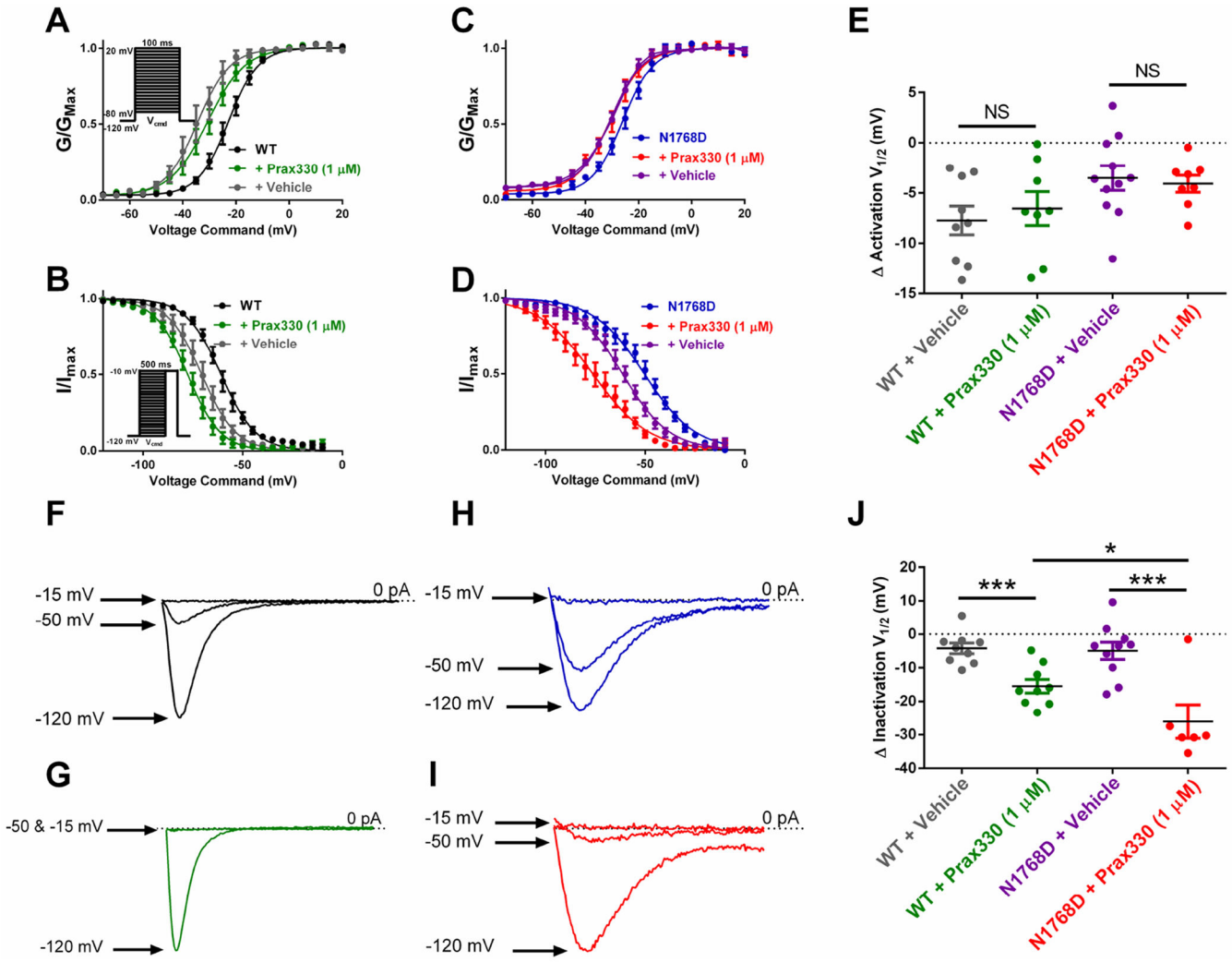

Figure 2. Prax330 hyperpolarizes steady-state inactivation curves in WT and N1768D $Na_V1.6$ channel currents.

A. Voltage-dependent activation curve for WT $Na_V1.6$ channel currents before (black), after treatment with Prax330 (gree; 1 μM; n=9), and vehicle control (gray; n=9). Inset shows voltage command protocol. Cells were held at −120 mV. **B.** Steady-state inactivation curves for WT $Na_v1.6$ channel currents before (black) and after treatment with Prax330 (green; 1 μM; n=9). Vehicle-treated controls are shown in gray (n=9). Inset shows voltage command protocol. Cells were held at −120 mV **C.** Voltage-dependent activation for N1768D $Na_V1.6$ channel currents before (blue) and after administration of Prax330 (red; 1 μM; n=8) or vehicle (purple; n=11). **D.** Steady-State inactivation for N1768D channel currents before (blue) and after treatment with Prax330 (red; 1 μM; n=6) or vehicle (purple; n=10). **E.** Activation half-maximal voltage ($V_{1/2}$) were not different between WT plus vehicle (gray; n=9) or WT plus Prax330 (1 μM; green, n=9), or N1768D plus vehicle (purple; n=11), and N1768D plus Prax330 (1 μM; red, n=8). Example traces of WT steady-state inactivation showing relative I_{NaT} after 500 ms pre-pulses to −120 mV, −50 mV, and −15 mV before **(F)** and after **(G)** treatment with Prax330 (1 μM). Example traces of N1768D steady-state

inactivation showing relative I_{NaT} after 500 ms pre-pulses to −120 mV, −50 mV, and −15 mV before **(H)** and after **(I)** treatment with Prax330 (1 μM). **J.** Hyperpolarizing shifts in steady-state inactivation $V_{1/2}$ for WT plus vehicle (gray; n=9), WT plus Prax330 (1 μM; green; n=9), N1768D plus vehicle (purple; n=10), and N1768D plus Prax330 (1 μM; red; n=6). Data shown as individual values and/or mean ± SEM. *P< 0.05, ***P<0.001.

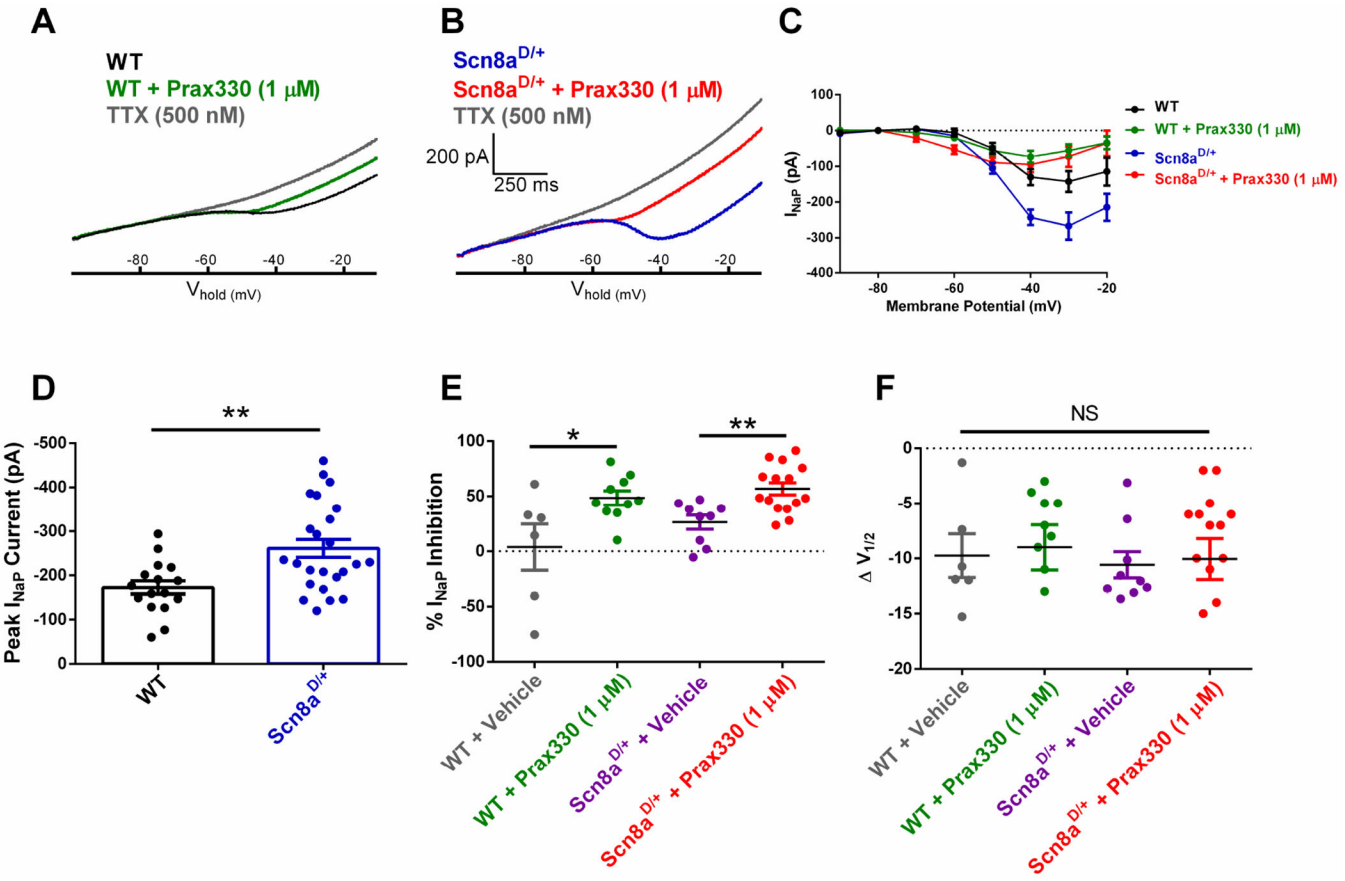

Figure 3. Prax330 (1 μM) inhibits I_{NaP} in subiculum pyramidal neurons.

A. Representative recording of I_{NaP} for WT before (black) and after (green) treatment with 1 μM Prax330 and 500 nM TTX (gray). **B.** Representative recording of I_{NaP} for *Scn8a*$^{D/+}$ before (blue) and after (red) treatment with 1 μM Prax330 and 500 nM TTX (gray). **C.** Current/voltage relationship of I_{NaP} for WT before (black) and after (green) Prax330 (1 μM) and current/voltage relationship of *Scn8a*$^{D/+}$ before (blue) and after (red) treatment with Prax330 (1 μM). **D.** Peak I_{NaP} current for WT (n=16 neurons, 7 mice) and Scn8a$^{D/+}$ (n=24 neurons, 8 mice) subiculum neurons. *Scn8a*$^{D/+}$ neurons have significantly larger peak I_{NaP}. **E.** Percent inhibition of I_{NaP} for WT plus vehicle (gray; n=6 neurons, 3 mice), WT plus Prax330 (1 μM; green; n=10 neurons, 4 mice), *Scn8a*$^{D/+}$ plus vehicle (purple; n=9 neurons, 3 mice), and *Scn8a*$^{D/+}$ plus Prax330 (1 μM; red, n=15 neurons, 5 mice). Compared to vehicle controls, Prax330 inhibited the steady-state I_{NaP} in both WT and *Scn8a*$^{D/+}$ subiculum neurons. **F.** Leftward shifts observed in activation $V_{1/2}$ were not different between WT, N1768D or their respective vehicle controls; WT plus vehicle (gray), WT plus Prax330 (1 μM; green), *Scn8a*$^{D/+}$ plus vehicle (purple), and *Scn8a*$^{D/+}$ plus Prax330 (1 μM; red). Data shown as individual values and/or mean ± SEM. *P<0.05, **P<0.01.

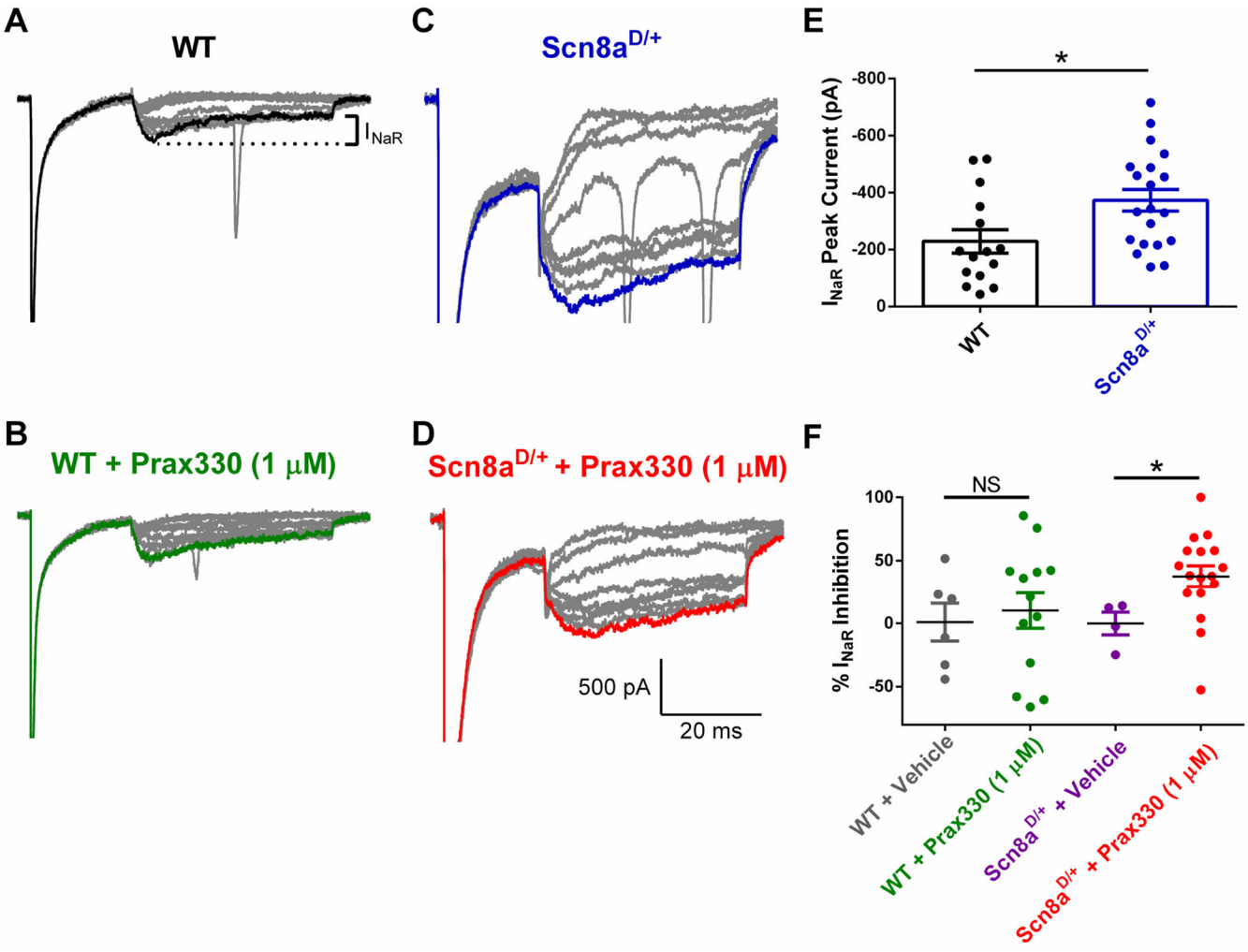

Figure 4. *Scn8a*$^{D/+}$ subiculum neuron I_{NaR} currents are inhibited by 1 μM Prax330.

A-B. Representative TTX-subtracted I_{NaR} traces for WT before **(A)** and after **(B)** treatment with Prax330 (1 μM). **C-D.** *Scn8a*$^{D/+}$ TTX-subtracted I_{NaR} traces before **(C)** and after **(D)** Prax330 1 μM treatment. **E.** Peak I_{NaR} for untreated WT (n=15 neurons, 8 mice) and *Scn8a*$^{D/+}$ (n=20 neurons, 7 mice). *Scn8a*$^{D/+}$ neurons have larger peak I_{NaR} compared to WT neurons. **F.** Percent inhibition of I_{NaR} for WT plus vehicle (gray; n=6 neurons, 3 mice), WT plus Prax330 (1 μM; green, n=13 neurons, 5 mice), *Scn8a*$^{D/+}$ plus vehicle (purple; n=4 neurons, 2 mice), and *Scn8a*$^{D/+}$ plus Prax330 (1 μM; red, n=13 neurons, 5 mice). Compared to vehicle controls, Prax330 did not inhibit the steady-state I_{NaP} in WT ($P>0.05$) but did inhibit I_{NaR} in *Scn8a*$^{D/+}$ neurons. Data shown as individual values and mean ± SEM. *$P<0.05$.

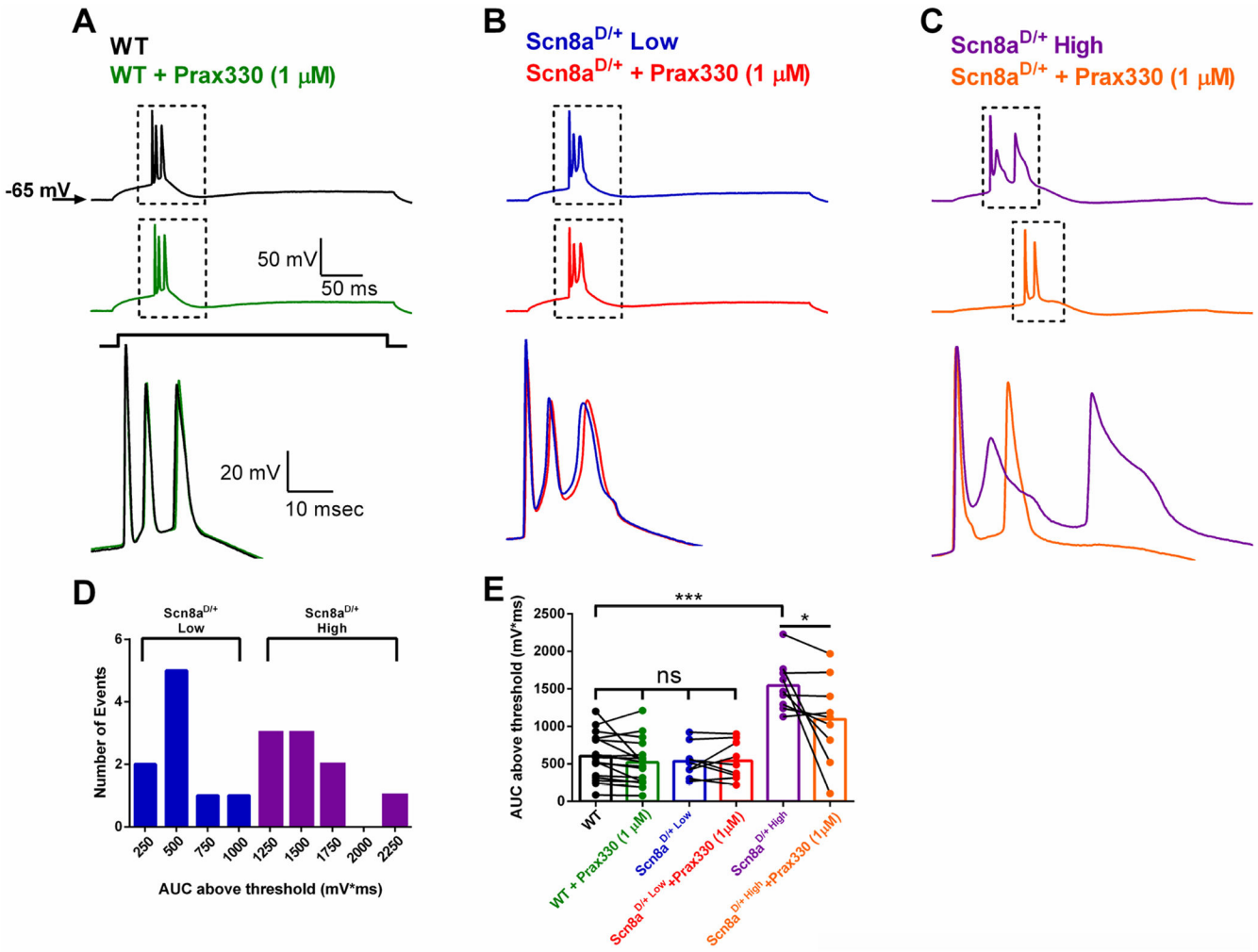

Figure 5. Prax330 preferentially suppresses aberrant AP-bursting in *Scn8a*$^{D/+}$ subiculum neurons.

A. Example traces for WT before (black) and after (green) treatment with Prax330 (1 μM). **B.** Example traces for a low bursting *Scn8a*$^{D/+}$ subiculum neuron before (blue) and after (red) treatment with Prax330 (1 μM). **C.** Example traces for an aberrant bursting *Scn8a*$^{D/+}$ subiculum neuron before (purple) and after (orange) treatment with Prax330 (1 μM). Note that Prax330 (1μM) preferentially reduces AUC in *Scn8a*$^{D/+}$-high bursting subiculum neurons (n=9 neurons, 7 mice) while having little effect on low bursting subiculum neurons (n=9 neurons, 7 mice), or WT neurons (17 neurons, 4 mice). **D.** Histogram of AUC data separated into *Scn8a*$^{D/+}$-low (blue) and *Scn8a*$^{D/+}$-high (purple) groups. **E.** Bar chart showing effects of Prax330 (1 μM) on AUC values. Data shown represent means and individual points before and after Prax330 treatment. *P<0.05, ***P<0.001.

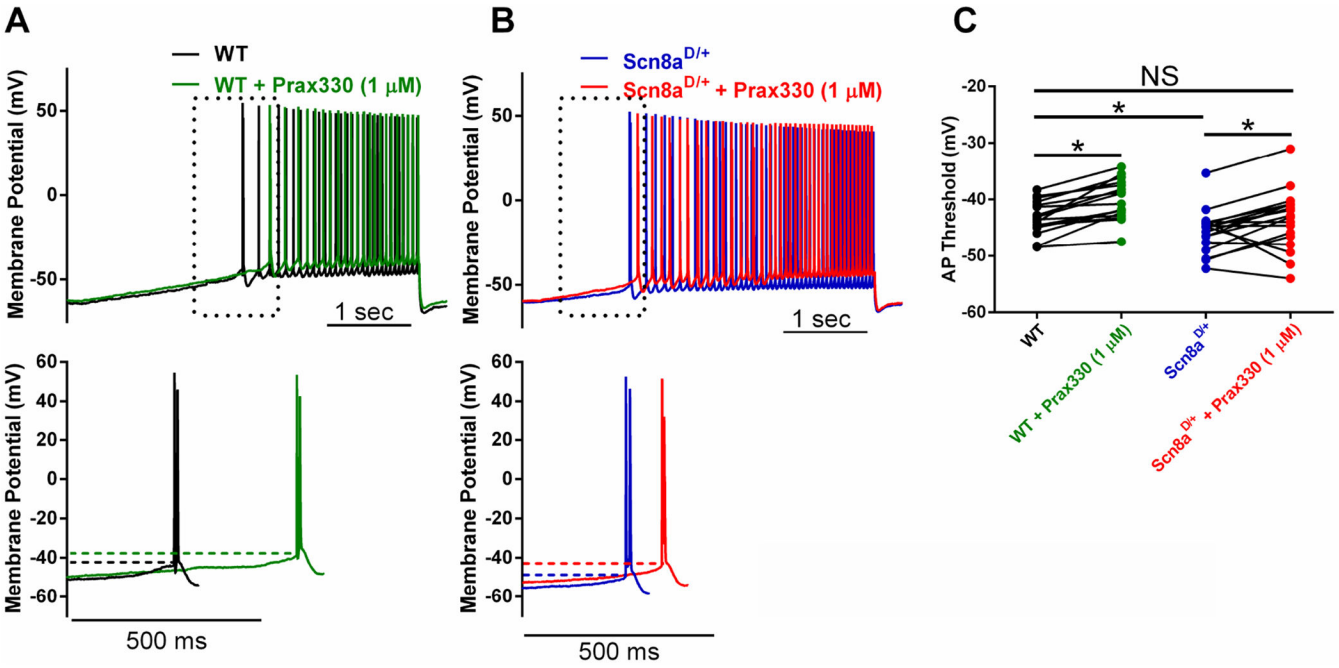

Figure 6. Prax330 rescues hyperpolarized AP threshold in *Scn8a*$^{D/+}$ subiculum neurons

A-B. Representative raw traces with APs evoked using a slow current injection ramp (100 pA/sec). **A. Top**. WT subiculum neuron before (black) and after (green) Prax330 (1 μM) treatment. **B**. **Top.** *Scn8a*$^{D/+}$ subiculum neuron before (blue) and after (red) treatment with Prax330 (1 μM). Lower panels in each case show expanded trace of first action potential. Dotted lines mark action potential threshold. **C.** Group data for action potential (AP) threshold for WT before (black) and after (green) treatment with 1 μM Prax330 (n= 17 neurons, 4 mice) and *Scn8a*$^{D/+}$ before (blue) and after (red) treatment with 1 μM Prax330 (n=18 neurons, 7 mice). Data shown represents individual points before and after Prax330 treatment. *P<0.05.

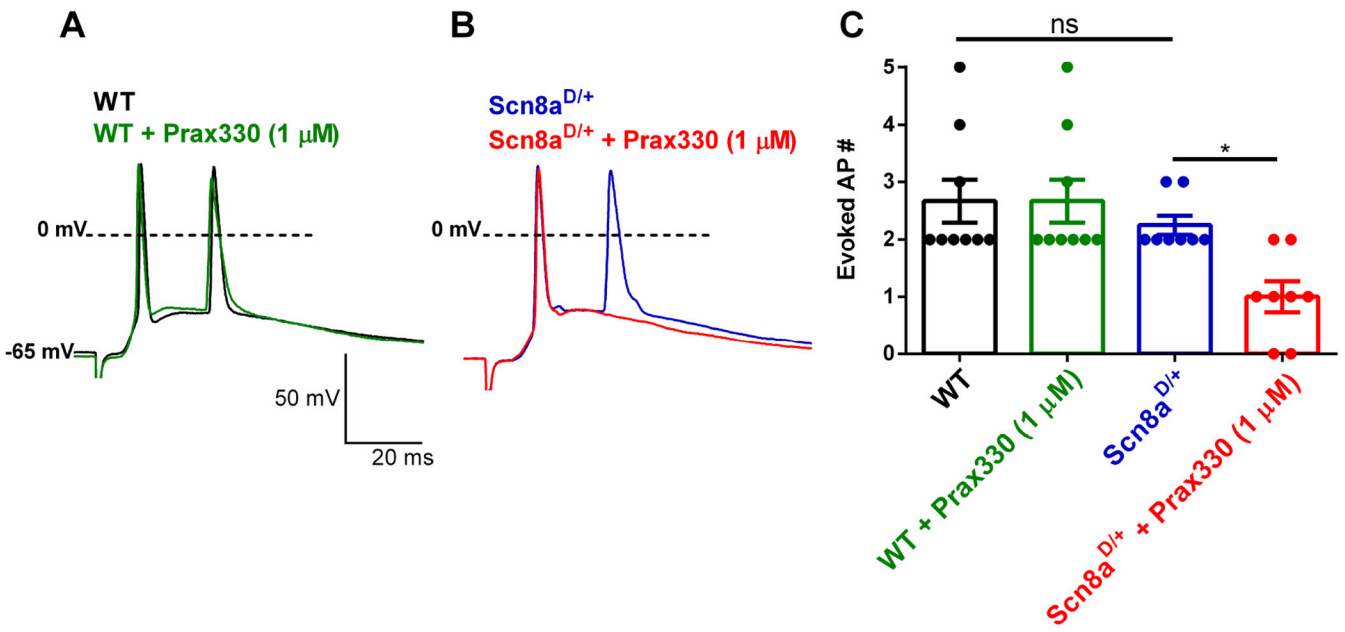

Figure 7. Prax330 reduces the number of synaptically-evoked burst APs in *Scn8a*$^{D/+}$ but not WT subiculum neurons.

A. Representative traces of WT (baseline, black; Prax330 (1 μM), green) demonstrates that Prax330 has no effect on the number of WT synaptically-evoked APs. **B.** Example traces of *Scn8a*$^{D/+}$ (baseline, blue; Prax330 (1 μM), red) demonstrates that Prax330 diminishes the number of *Scn8a*$^{D/+}$ synaptically-evoked APs. **C.** Bar chart demonstrating effects of Prax330 (1 μM) on WT and *Scn8a*$^{D/+}$ synaptically-evoked APs (n=9 neurons from 4 WT mice and n=8 neurons from 4 *Scn8a*$^{D/+}$ mice). Data shown represent individual points and means ± S.E.M. *P<0.05.

TABLE 1.

Effect of Prax330 (1 μM) on WT and N1768D $Na_V1.6$ sodium currents

	Activation		Inactivation	
	$V_{1/2}$ (mV)	k	$V_{1/2}$ (mV)	k
WT	−22.7 ± 1.5	4.9 ± 0.3	−60.9 ± 1.8	8.0 ± 0.3
+ Vehicle	−35.0 ± 2.0	5.3 ± 0.7	−67.8 ± 2.0	7.6 ± 0.3
+ Prax330 (1 μM)	−30.4 ± 2.4	5.3 ± 0.7	−77.3 ± 2.4*	7.7 ± 0.3
N1768D	−25.6 ± 1.4	5.6 ± 0.5	−50.8 ± 2.6#	12.8 ± 1.3#
+ Vehicle	−32.6 ± 1.0	6.4 ± 0.5	−62.0 ± 2.3	10.8 ± 0.9
+ Prax330 (1 μM)	−30.2 ± 1.7	6.0 ± 0.5	−76.9 ± 3.7*	12.4 ± 0.9

* indicates p<0.05 comparing vehicle and Prax330 application using unpaired t-test.

# indicates p<0.05 comparing WT and N1768D groups using unpaired t-test.

TABLE 2.

Effect of Prax330 on passive and active membrane properties in WT and Scn8a$^{D/+}$ subiculum neurons.

	Threshold (mV)	Input Resistance (MΩ)	Rheobase (pA)	Amplitude (mV)	Upstroke Velocity (mV/ms)	Downstroke Velocity (mV/ms)	APD50 (ms)
WT	−43.2 ± 0.8	103 ± 7	213 ± 8	93.9 ± 1.9	335 ± 26	−80 ± 2.9	1.05 ± 0.04
+ Prax330 (1 μM)	−40.1 ± 0.9 *	112 ± 9	214 ± 14	85.6 ± 2.8 *	277 ± 22**	−74 ± 4.6	1.11 ± 0.06
Scn8a$^{D/+}$	−46.2 ± 0.6 #	153 ± 17 #	101 ± 8	96.2 ± 2.4	336 ± 15	−56.3 ± 2.9 #	1.37 ± 0.08 #
+ Prax330 (1μM)	−43.6 ± 1.2 *	147 ± 24	128 ± 11 *	90.9 ± 1.9 *	278 ± 15 *	−58.4 ± 3.6	1.40 ± 0.11

* indicates p<0.05 comparing within cell (before and after Prax330 application) using paired t-test.

# indicates p<0.05 comparing WT and *Scn8a*$^{D/+}$ groups using unpaired t-test.